Development 134, 2913-2923 (2007) doi:10.1242/dev.002576

EGFL7 regulates the collective migration of endothelial cells by restricting their spatial distribution

Maike Schmidt[1], Kim Paes[2], Ann De Mazière[3], Tanya Smyczek[1], Stacey Yang[1], Alane Gray[4], Dorothy French[5], Ian Kasman[5], Judith Klumperman[3], Dennis S. Rice[2] and Weilan Ye[1,*]

During sprouting angiogenesis, groups of endothelial cells (ECs) migrate together in units called sprouts. In this study, we demonstrate that the vascular-specific secreted factor EGFL7 regulates the proper spatial organization of ECs within each sprout and influences their collective movement. In the homozygous *Egfl7*-knockout mice, vascular development is delayed in many organs despite normal EC proliferation, and 50% of the knockout embryos die in utero. ECs in the mutant vasculatures form abnormal aggregates and the vascular basement membrane marker collagen IV is mislocalized, suggesting that ECs fail to recognize the proper spatial position of their neighbors. Although the migratory ability of individual ECs in isolation is not affected by the loss of EGFL7, the aberrant spatial organization of ECs in the mutant tissues decreases their collective movement. Using in vitro and in vivo analyses, we showed that EGFL7 is a component of the interstitial extracellular matrix deposited on the basal sides of sprouts, a location suitable for conveying positional information to neighboring ECs. Taken together, we propose that EGFL7 defines the optimal path of EC movement by assuring the correct positioning of each EC in a nascent sprout.

KEY WORDS: ECM, EGFL7, Migration, Morphogenesis, Vascular, Mouse

INTRODUCTION

Cell migration is an important aspect in many physiological and pathological processes. In multicellular organisms, although cells can migrate individually (Rembold et al., 2006), it is more common that cells migrate in groups (Haas and Gilmour, 2006). Depending on the tissue architecture, a cohort of migrating cells can assume different shapes, such as sheets, chains or tubes (Friedl et al., 2004). Many questions concerning collective cell migration have yet to be answered. For example, how does a group of cells maintain a defined organization as they move? How is the size of a group of migrating cells regulated? Does the spatial organization of the migrating cells influence their migration speed? Answering these questions will not only help us understand the basis of tissue morphogenesis, but might also help us design ways to interfere with pathological conditions that involve collective cell migration, such as tumor angiogenesis. Using sprouting angiogenesis during embryonic and neonatal development as a model, we attempted to answer some of these questions.

Vascular development in embryonic and postnatal life is a spatially and temporally orchestrated process, as many steps in vasculogenesis and angiogenesis are coordinated by factors present in the microenvironment (Flamme et al., 1997; Rossant and Howard, 2002; Yancopoulos et al., 2000). For example, endothelial cell (EC) migration is often guided by factors produced by the target tissues (Carmeliet and Tessier-Lavigne, 2005; Coultas et al., 2005; Eichmann et al., 2005). The cellular events related to EC migration in response to external cues are most extensively documented during sprouting angiogenesis, which is a means of creating new vessels from existing ones (Gerhardt and Betsholtz, 2005; Patan, 2004). It is generally believed that tip cells, which are the specialized ECs situated at the tips of sprouts, respond to chemoattractants and migrate actively along extracellular matrix (ECM) rails; whereas the stalk cells – ECs that line the wall of a nascent vessel – are pulled forward passively by the tip cells (Davis and Senger, 2005). Stalk cell proliferation contributes to the extension of sprouts (Gerhardt and Betsholtz, 2005; Gerhardt et al., 2003), but it is not clear if stalk cells can influence the movement of a sprout in other ways. In this study, we provide evidence to suggest that the spatial organization of the stalk cells contributes to the collective EC movement, and show that this process is regulated by the vascular-specific secreted factor EGFL7.

EGFL7 is a secreted factor that is specifically expressed by ECs (Campagnolo et al., 2005; Fitch et al., 2004; Parker et al., 2004; Soncin et al., 2003) (see also Fig. S2 in the supplementary material). Expression is high during embryonic and neonatal development in all vessel types. As the vasculatures mature, *Egfl7* expression is downregulated in many vessels. In contexts requiring new vessel growth, such as tumorigenesis or vascular injury, *Egfl7* levels increase again (Campagnolo et al., 2005; Parker et al., 2004). In zebrafish embryos, Egfl7 is required for the midline angioblasts to disperse along the dorsal-ventral axis, which is an essential step in axial vessel tubulogenesis (Parker et al., 2004). Owing to the strong defect in vasculogenesis, we were unable to investigate the role of *Egfl7* in angiogenesis using zebrafish embryos because axial vessel assembly precedes and impacts sprouting angiogenesis (Kidd and Weinstein, 2003). In this study, we describe a unique role that EGFL7 plays in regulating sprouting angiogenesis and vascular patterning.

MATERIALS AND METHODS

Generation of *Egfl7*$^{-/-}$ mice

The insertional knockout line was generated as described (Zambrowicz et al., 2003; Zambrowicz et al., 1998). The homologous recombination line was generated following standard techniques (see Fig. S1 in the supplementary material).

[1]Tumor Biology and Angiogenesis Department, Genentech Inc., 1 DNA Way, South San Francisco, CA 94080, USA. [2]Lexicon Genetics Inc., 8800 Technology Forest Place, The Woodlands, TX 77381-1160, USA. [3]Cell Microscopy Center, Department of Cell Biology, University Medical Center Utrecht and Institute for Biomembranes, 3584CX, Utrecht, Netherlands. [4]Translational Oncology Department and [5]Pathology Department, Genentech Inc., 1 DNA Way, South San Francisco, CA 94080, USA.

*Author for correspondence (e-mail: loni@gene.com)

Accepted 30 May 2007

Histology and immunostaining

Primary antibodies: αSMA (Sigma), BrdU (Serotec), activated caspase 3 (BioVision), CD31 (BD), type IV collagen (CosmoBio), FAK (Calbiochem), FAKpY397 (Upstate), FAKpY861 (BioSource), fibronectin (NeoMarkers), GFAP (NeoMarkers), Ki67 (Chemicon), NG2 (Chemicon), VE-cadherin (cadherin 5) (BD), VEGF (RDI), EGFL7 (Genentech) (Parker et al., 2004) and Isolectin B4 (Sigma).

Wholemount immunohistochemistry (IHC) and immunofluorescence (IF) were performed as described (http://spot.colorado.edu/~klym/) (Gerhardt et al., 2003).

For BrdU labeling, animals were injected i.p. with 100 μg BrdU/g, 2 hours prior to sacrifice. For vessel perfusion, adult animals were injected with FITC-conjugated tomato lectin (Vector) into the tail vein (150 μl at 1 mg/ml per mouse), whereas neonatal animals were injected via the intracardiac route under anesthesia.

Hypoxia was detected using the Hypoxyprobe-1 Plus Kit following manufacturer's instruction (Chemicon).

For Hematoxylin and Eosin (H&E) and IHC staining on tissue sections, tissues were fixed with Bouin's. For IF, tissues were fixed with 4% paraformaldehyde/PBS for the majority of markers, or unfixed for the anti-EGFL7. For β-galactosidase staining, tissues were fixed in 0.25% glutaraldehyde/PBS for 15 minutes.

Angiography

Fluorescent angiography was performed as described (Rice et al., 2004).

Electronmicroscopy analysis

Neonates were perfused under anesthesia with PBS/heparin, followed by half-strength Karnovsky fixative. After further fixation, retinas were excised in 0.1 M Na cacodylate buffer (pH 7.4), and processed for Epon embedding following standard protocols. A quarter of each retina was stained with Isolectin B4 to allow monitoring of vascular progression.

EGFL7 subcellular localization

Human umbilical vein endothelial cells (HUVECs, Cambrex) were seeded onto chamber slides (Nunc) precoated with 5 μg/ml fibronectin (Sigma), type IV collagen, type I collagen (BD) or laminin (Invitrogen), or co-cultured with human dermal fibroblasts (Clonetics) in EGM2 medium (Cambrex). After 3-6 days in culture, cells were incubated for 20 minutes in EGM2 medium with 5% BSA (Roche) and complete protease inhibitor (Roche). EGFL7 antibody (10 μg/ml, Genentech) was added and incubated for 1 hour. Cells were stained with secondary antibody in detergent-free buffers.

Chicken embryonic fibroblasts (CEFs) were transfected with plasmids encoding the HA-tagged full-length human EGFL7 or GFP in the RCAS vector. CEFs were grown in 10 ml serum-free culture medium on a 10 cm plate for 2 days at confluent density. Conditioned media were harvested and concentrated to 1 ml. Cells were washed and incubated for 15 minutes at 37°C with 1 ml 1 M NaCl (high salt extract), lysed in 1 ml cold 0.5% deoxycholate (DOC) in PBS for 15 minutes on ice (cell lysate extract). Plates were washed several times with PBS to remove all cells, and 1 ml of the ECM-extraction buffer (5% SDS, 100 mM Tris, pH 6.8) was added for 15 minutes. ECM was scraped from the plate and heated at 96°C for 10 minutes. An equal volume of each fraction was analyzed by western blotting with an anti-HA antibody (Covance).

VEGF ELISA

Whole retinas were collected at P5 and P8. VEGF levels in the homogenized tissues were quantified by ELISA following the manufacturer's instructions (Quantikine).

Endothelial cell isolation from mouse tissue

Mice (8 to 12 weeks old) were anesthetized and perfused with 0.05% collagenase/HBSS. ECs were isolated from the liver using biotinylated anti-CD31 antibody (BD) and streptavidin microbeads (MACS system, Miltenyi Biotec). An aliquot of cells was stained with anti-VE-cadherin (BD) to evaluate purity.

Aortic ring explants

Thoracic aortae were excised from mice used for EC isolation (see method above), immediately after perfusion. Aortae were cleaned of all connective tissue and cut into 1- to 2-mm-thick rings. Rings were embedded in rat tail type I collagen (BD) and cultured for several days in EGM2 medium (Cambrex) plus 3% mouse serum (Taconic). Live rings were imaged using an inverted microscope from days 4-7. Some rings were fixed at day 6 for marker analysis.

Trans-well migration assay

Trans-well inserts (BD) were coated overnight with 8 μg/ml fibronectin (Roche) or EGFL7 (Genentech). Mouse ECs isolated from liver were plated in EBM medium (Cambrex), 0.1% BSA at 10^6 cells/well. After overnight incubation with 10 ng/ml VEGF in the lower chamber, cells were fixed with methanol and stained with Sytox Green (Invitrogen). Nuclei on the bottom of the insert were counted.

HUVEC random migration stimulated by HGF

Chamber slides were coated overnight with 5 μg/ml indicated proteins. After blocking with BSA, HUVECs were seeded sparsely and cultured in EGM2 medium containing 100 ng/ml HGF. Bright-field images were collected every 8 minutes for 24 hours. Individual cell migration over this time frame was analyzed by object tracking (Metamorph).

Quantification methods

For a detailed explanation of the quantification methods employed, see Fig. S4 in the supplementary material.

RESULTS

Targeted inactivation of *Egfl7* results in reduced viability

We generated two independent mouse lines with an *Egfl7* deletion. The first line was derived from a random mutagenesis screen using a retroviral gene trap vector (Zambrowicz et al., 1998). Vector insertion occurred in intron 2, upstream of the translation initiation codon in exon 3 (see Fig. S1A in the supplementary material), which leads to silencing of endogenous *Egfl7* transcription (Fig. S1B in the supplementary material), thus abolishing EGFL7 translation (Fig. 7L,M and see Fig. S1C in the supplementary material). We also generated an *Egfl7* mutant line by homologous recombination that removes exons 5-7 (see Fig. S1D in the supplementary material) and introduces a premature stop codon, thereby producing a truncated protein with an incomplete EMI domain that terminates at Tyr90. Loss of EGFL7 protein was confirmed by immunofluorescence staining on frozen tissues from the wild-type ($Egfl7^{+/+}$) and homozygous ($Egfl7^{-/-}$) littermates (see Fig. S1G in the supplementary material). We found that the phenotypes were consistent between the two mutant lines, confirming that the biological activities described in this study are attributable to the EGFL7 protein. Because of space limitations, data presented in the main text are from the insertional line unless specified otherwise, and most of the data from the homologous recombination line are presented in the supplementary material.

$Egfl7^{-/-}$ mice are born with a substantially reduced mendelian ratio, whereas the mendelian ratio for embryos analyzed at 9.5-11.5 dpc (E9.5-11.5) was normal (Table 1). Between E13.5 and E15.5, a significant number of $Egfl7^{-/-}$ embryos had severe systemic oedema (Fig. 1A-D, Table 2), and a subset of the oedematous embryos had no heartbeat at E14.5 and E15.5 (Table 2). These analyses indicate that ~50% of the $Egfl7^{-/-}$ embryos die in utero. Lethality probably occurs at around E14.5-15.5.

The surviving $Egfl7^{-/-}$ mice gained weight at a normal pace (Fig. 1E) and their tissues had normal histology (Fig. 1F-M). The knockout males and females were fertile, and females were capable

Table 1. Mendelian ratios of the *Egfl7*-knockout lines

Knockout line	Genetic background (generation)	Age	Ratios for each genotype: Observed % (*n*) Genotype +/+	+/–	–/–	Expected % (*n*) Genotype +/+	+/–	–/–	Total number of animals analyzed (*n*)	*P* values of observed vs expected (–/–) ratios (χ^2 test)
Insertional knockout	129svj/C57Bl/6 mixed	Adult	33.1 (115)	53.3 (185)	**13.5** (47)	25 (87)	50 (173)	25 (87)	347	**<0.0001***
	129svj/C57Bl/6 mixed	P0-8	33.2 (68)	53.7 (110)	**13.1** (27)	25 (51)	50 (103)	25 (51)	205	**<0.0001***
	129svj/C57Bl/6 mixed	E9.5-15.5	24 (62)	51.2 (132)	24.8 (64)	25 (64.5)	50 (129)	25 (64.5)	258	0.9185
Homologous recombination knockout	C57Bl/6 (N5)	Adult	33.9 (96)	52 (147)	**14.1** (40)	25 (71)	50 (141)	25 (71)	283	**<0.0001***
	C57Bl/6 (N10)	Adult	31.5 (73)	59 (137)	**9.5** (22)	25 (58)	50 (116)	25 (58)	232	**<0.0001*** (0.0921 N10 vs N5)
	129svj Pure	Adult	36.6 (30)	48.8 (40)	**14.6** (12)	25 (20.5)	50 (41)	25 (20.5)	82	**0.0188***
	C57Bl/6 (N5)	P0-8	31.7 (91)	54.7 (157)	**13.6** (39)	25 (72)	50 (143)	25 (72)	287	**<0.0001***
	C57Bl/6 (N0-5)	E9.5-15.5	28.5 (84)	46.1 (136)	25.4 (75)	25 (74)	50 (147)	25 (74)	295	0.3104

The offspring of multiple pairs of *Egfl7*$^{+/-}$ parents in different genetic background were genotyped and counted. The N values refer to how many generations the mutant mice in the 129svj/C57Bl/6 mixed background have been crossed to C57Bl/6 mice. Values in bold are statistically significant (*).

of supporting the growth of full-size litters (Table 3). However, low-level sporadic hypoxia was seen in many organs from the *Egfl7*$^{-/-}$ adult mice (*n*=2, age=4 months), including retina, heart, pancreas, crypts of the intestinal villi, kidney medulla and adipose tissues (Fig. 1J-M and data not shown). In the *Egfl7*$^{+/+}$ littermates (*n*=2), hypoxic signals in the aforementioned tissues were very low (Fig. 1F) or absent (Fig. 1G-I). However, variable hypoxyprobe signals were seen in the liver, kidney cortices and in the tips of the intestinal villi in both *Egfl7*$^{+/+}$ and *Egfl7*$^{-/-}$ mice (data not shown), making evaluation in these tissues difficult. Interestingly, hypoxia was not detected in the lungs of either genotype (data not shown), presumably owing to high oxygen content in this organ. Despite tissue hypoxia, the *Egfl7*$^{-/-}$ mice and their *Egfl7*$^{+/+}$ siblings had a similar life span (data not shown).

Loss of *Egfl7* leads to delayed vascular development in multiple organs

Vascular development defects were observed in many tissues in the *Egfl7*$^{-/-}$ embryos and neonates. For ease of description, we chose three vasculatures as examples: the embryonic coronary, the

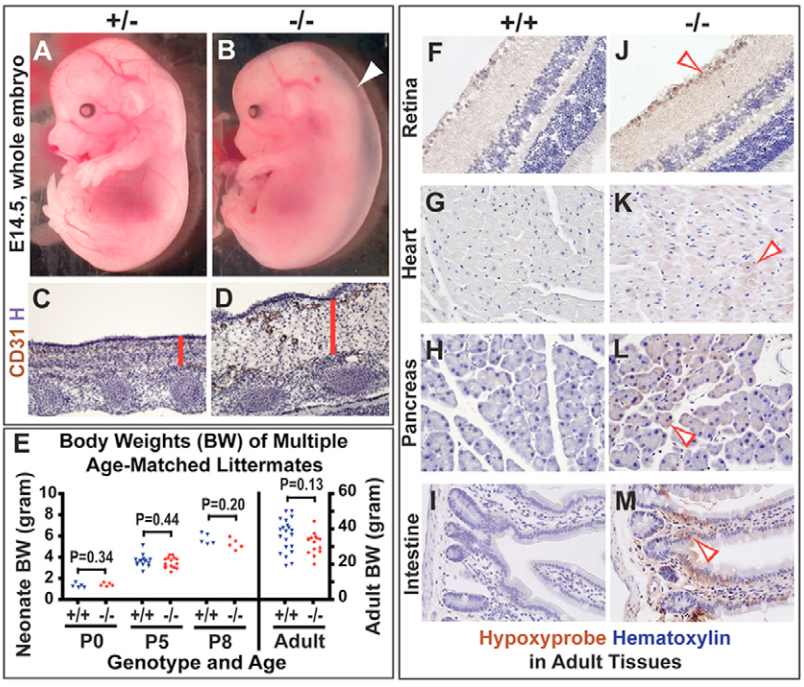

Fig. 1. General phenotypes of the *Egfl7*-knockout mouse. (**A**,**B**) *Egfl7*$^{+/-}$ (A) and *Egfl7*$^{-/-}$ (B) E14.5 littermates. Arrowhead indicates systemic oedema in the *Egfl7*$^{-/-}$ mouse. (**C**,**D**) CD31 [also known as PECAM1; brown, endothelial cell (EC) marker] and Hematoxylin (blue, H, nuclear marker) staining on transverse sections of the neck dermis from *Egfl7*$^{+/+}$ (C) and *Egfl7*$^{-/-}$ (D) E14.5 littermates. Red bars indicate the thickness of the epidermis. Increased thickness in the *Egfl7*$^{-/-}$ tissue is a hallmark of oedema. (**E**) Body weights of multiple pairs of *Egfl7*$^{+/+}$ and *Egfl7*$^{-/-}$ littermates at the indicated ages. Adults are all between 4-7 months. *P* values are calculated with unpaired, two-tailed *t*-test with 95% confidence interval (the same method is used for all *P* values unless specified otherwise). (**F-M**) Hypoxyprobe (brown) and Hematoxylin (blue) staining on sections of adult organs from *Egfl7*$^{+/+}$ and *Egfl7*$^{-/-}$ littermates. Genotype and organ names are indicated. Arrowheads indicate example hypoxic cells. The actual size represented by the width of the panel: 8.5 mm (A,B); 0.87 mm (C,D); 430 μm (F-M).

Table 2. Summary of the embryonic phenotypes in the *Egfl7*-knockout line*

Age	Total number of embryos analyzed	Phenotypic category in the *Egfl7*$^{-/-}$ embryos % (*n*)				Phenotypic category in the *Egfl7*$^{+/+}$ and *Egfl7*$^{+/-}$ embryos % (*n*)			
		No observed phenotype	Systemic oedema	No heart beat and systemic oedema	Number of *Egfl7*$^{-/-}$ embryos	No observed phenotype	Systemic oedema	No heart beat	Number of *Egfl7*$^{+/+}$ and *Egfl7*$^{+/-}$ embryos
E9.5-12.5	109	100 (19)	0 (0)	0 (0)	19	98.9 (89)	0 (0)	1.1 (1†)	90
E13.5	35	44.4 (4)	**55.6 (5)**	0 (0)	9	96.2 (25)	0 (0)	3.8 (1‡)	26
E14.5	93	45.5 (15)	**39.3 (13)**	**15.2 (5)**	33	100 (60)	0 (0)	0 (0)	60
E15.5	21	33.3 (1)	0 (0)	**66.7 (2)**	3	100 (18)	0 (0)	0 (0)	18

Values in bold are statistically significant.
*Insertional knockout in the 129svj/C57Bl/6 mixed background.
†This is an *Egfl7*$^{+/+}$ E12.5 embryo. It did not have oedema.
‡This is an *Egfl7*$^{+/-}$ embryo. It did not have oedema.

neonatal retinal, and the embryonic cranial vasculatures. The common feature among these three systems is that they develop in a well-defined spatiotemporal pattern.

The coronary vascular plexus originates from the atrial-ventricular and interventricular grooves at ~E11.5, and extends downward and outward to cover the entire epicardium by E14.5 (Lavine et al., 2006). Loss of EGFL7 resulted in a significant delay in this sequence of events. The degrees of coronary vascular coverage were significantly reduced in ~50% of the *Egfl7*$^{-/-}$ embryos at E12.5 and E14.5 (Fig. 2A-D,G).

The development of the retinal vasculature also follows a precise temporal schedule (Benjamin et al., 1998; Dorrell and Friedlander, 2006; Stone et al., 1995). Vascularization in the retina commences at postnatal day 0 (P0), when ECs from the central retinal artery begin to migrate outward to the periphery within the nerve fiber layer (NFL), and vascular coverage of the NFL completes around P8-9. In 100% of *Egfl7*$^{-/-}$ mice, the centrifugal expansion of the NFL vascular plexus across the retina was impaired. This delay was evident as early as P2 and persisted until P11 (Fig. 2I-O and see Fig. S3C-G in the supplementary material; data not shown). Interestingly, retinal sizes were unaffected despite the vascular coverage defect, possibly owing to the slow growth of this organ (Fig. 2P and see Fig. S3H in the supplementary material).

Cranial vascular development is also easy to follow in the mouse embryo. At ~E10, the superficial cranial vessels develop by sprouting from the cardinal vein. The subsequent rostral migration

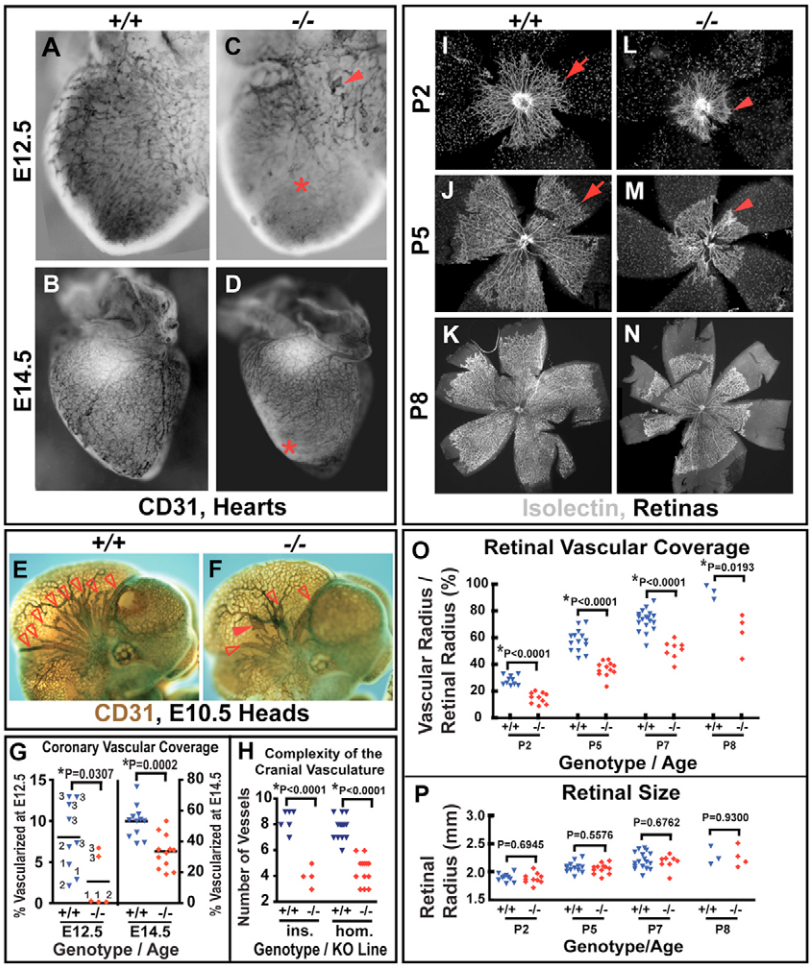

Fig. 2. Loss of *Egfl7* results in delay of vascularization. (**A-D**) CD31 wholemount staining on embryonic mouse hearts from *Egfl7*$^{+/+}$ (A,B) and *Egfl7*$^{-/-}$ (C,D) littermates at E12.5 (A,C, dorsal view of the left ventricles) and E14.5 (B,D, lateral view of the left ventricles, dorsal is to the right). Asterisks, areas without coronary vasculature; weak signal is from the underlying endocardium. (**E**,**F**) CD31 wholemount staining on embryonic heads from *Egfl7*$^{+/+}$ (E) and *Egfl7*$^{-/-}$ (F) littermates at E10.5. Open arrowheads, major cranial vessels. (**G**) Ventral coronary vascular coverage of multiple pairs of *Egfl7*$^{+/+}$ and *Egfl7*$^{-/-}$ littermates at E12.5 and E14.5. Horizontal bars represent means. Because of large inter-litter variation at E12.5, littermate relationship is specified with numbers in the graph. Significant difference is marked with an asterisk next to each *P* value. (**H**) Major cranial vessel counts of multiple pairs of *Egfl7*$^{+/+}$ and *Egfl7*$^{-/-}$ E10.5 littermates from two knockout lines. ins, insertional knockout line; hom, homologous recombination knockout line. (**I-N**) Isolectin B4 (EC marker) staining on flatmount neonatal retinas from *Egfl7*$^{+/+}$ (I-K) and *Egfl7*$^{-/-}$ (L-N) littermates at P2 (I,L), P5 (J,M) and P8 (K,N). (**O**,**P**) Retinal vascular coverage (O) and size (P) of multiple pairs of *Egfl7*$^{+/+}$ and *Egfl7*$^{-/-}$ newborn littermates at the indicated ages. Solid red arrowheads indicate example aberrant EC clusters; arrows indicate sprouts at the retinal vascular migration front. The actual size represented by the width of the panel: 0.9 mm (A,C); 1.4 mm (B,D); 3.6 mm (E,F); 3 mm (I,J,L,M); 4.7 mm (K,N); K and N are assembled from overlapping 4× images.

Table 3. Fertility of *Egfl7*-knockout adult mice

Egfl7 genotype of the parents		Number of litters	Average litter size	*P* value (*t*-test) between these two cohorts
Male	Female			
–/–	+/–	10	6.4	0.65
+/–	–/–	4	5.8	0.65

and branching of these vessels give rise to an elaborate vasculature that covers a significant portion of the lateral midbrain by E11.5 (Fiore et al., 2005). The development of the cranial vascular bed was delayed in the absence of EGFL7, as vascular complexity was reduced in the heads of the *Egfl7*$^{-/-}$ embryos (Fig. 2E,F,H and see Fig. S3A,B in the supplementary material).

In all three vasculatures, aberrant EC clusters were observed (solid arrowheads in Fig. 2 and Fig. S3 in the supplementary material).

Loss of *Egfl7* causes vascular morphological alterations in the surviving mice

Despite the significant delay in vascular development in many organs, ~50% of the *Egfl7*$^{-/-}$ mice survived (Table 1), and all of the surviving mice had vascular coverage in all the organs that we examined (Fig. 3 and data not shown). However, the morphology and organization of these vasculatures were altered in more than 80% of the *Egfl7*$^{-/-}$ mice. The most prominent vascular phenotypes found in these mice were: tortuosity (Fig. 3C,N and see Fig. S3K,O,R in the supplementary material); irregular diameters (Fig. 3G-K and see Fig. S3P,S in the supplementary material); and clustering of multiple vessels (arrows in Fig. 3 and Fig. S3K,P-Q in the supplementary material).

The presence of tissue hypoxia (Fig. 1) and vascular morphological defects suggest that the vasculatures in the mutant adult mice might not function optimally.

The vascular development phenotype is a primary defect in the endothelium

In order to understand the cellular mechanism of the phenotypes described above, we addressed several questions:

First, we investigated whether the vascular phenotypes are caused by defects outside of the vasculature. We found no obvious defects in a number of cell types closely associated with the vasculature, and the expression of VEGFA and fibronectin – two factors that are relevant to retinal vascular development – was unchanged in the *Egfl7*$^{-/-}$ tissues (see Figs S5, S6 in the supplementary material). Together with the fact that EGFL7 expression has not been found outside of the vascular endothelium, we conclude that the vascular defects are primary.

Second, we examined whether the reduced vascular coverage in the neonatal retinas is due to a reduction in EC proliferation by carrying out in vivo BrdU labeling and Ki67 staining. Our results indicated that EC proliferation is not altered in the *Egfl7*$^{-/-}$ retina at any of the postnatal stages examined (see Fig. S7A-C in the supplementary material; data not shown). This conclusion is further supported by the analysis of primary ECs isolated from the *Egfl7*$^{-/-}$ and *Egfl7*$^{+/+}$ littermates and cultured in vitro (see Fig. S7F in the supplementary material).

Third, we asked whether reduced vascular coverage in the neonatal retinas is due to altered EC apoptosis during postnatal development. Immunostaining of activated caspase 3 on retinal sections (see Fig. S7D,E in the supplementary material) revealed minimal retinal EC apoptosis at P2, regardless of the *Egfl7* genotype.

EGFL7 regulates the collective movement of ECs during sprouting angiogenesis

The results described in the previous section prompted us to investigate whether EC migration is altered in the *Egfl7*$^{-/-}$ tissues. Since delayed sprouting angiogenesis is evident in multiple mutant organs, we decided to use aortic ring culture, which is a sprouting angiogenesis model that can be followed temporally. Using live imaging, we monitored numerous sprouts individually over a period of 4 days in rings isolated from *Egfl7*$^{+/+}$ and *Egfl7*$^{-/-}$ littermates, and saw a significant reduction in sprout extension velocity in the knockout rings (Fig. 4A-D).

We also sought additional, but less direct, evidence for the alteration of EC motility. Focal adhesion kinase (FAK; also known as PTK2 – Mouse Genome Informatics) phosphorylation was chosen because this is an important event required for cells to adhere to and migrate on ECM substrates (Parsons, 2003). We found that phosphorylation on tyrosine 861 (pY861) is the predominant form in ECs in the wild-type neonatal retinas and aortic rings (see Fig. S8A,B,I,J in the supplementary material), whereas significant reduction of FAK-pY861 occurred in the *Egfl7*-deficient stalk cells in these two tissues (see Fig. S8C,D,K,L in the supplementary

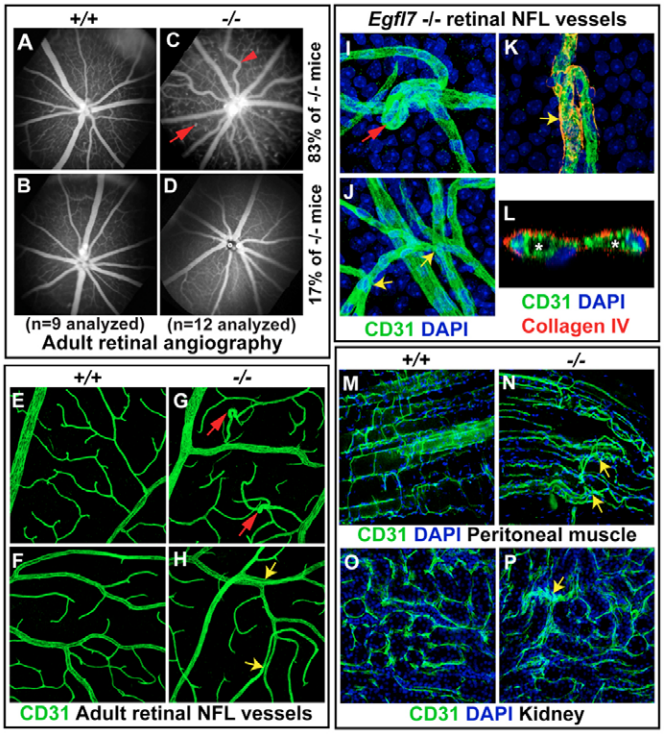

Fig. 3. Vascular phenotypes in the adult *Egfl7*-knockout mouse. (**A-H**) Fluorescent angiography (A-D) and CD31 fluorescent staining (E-H) in the retinas of multiple pairs of *Egfl7*$^{+/+}$ (A,B,E,F) and *Egfl7*$^{-/-}$ (C,D,G,H) littermates. (**I-L**) High-magnification views of aberrant structures in the *Egfl7*$^{-/-}$ retinas. L is a *z*-section showing two juxtaposed vessels. Blue, DAPI (I-L, nuclear marker); green, CD31 (I-L); red, collagen IV (K,L only, vascular basement membrane marker). (**M-P**) CD31 staining on 50 μm-thick sections of peritonea (M,N) and kidney (O,P) from *Egfl7*$^{+/+}$ (M,O) and *Egfl7*$^{-/-}$ (N,P) littermates. Arrowhead, tortuous vessels; red arrows, knots formed by multiple vessels; yellow arrows, vessels of similar diameter running close to each other; asterisks, vascular lumen. The actual size represented by the width of the panel: 1.2 mm (A-D); 330 μm (E-H); 88 μm (I-K); 25 μm (L); 275 μm (M-P).

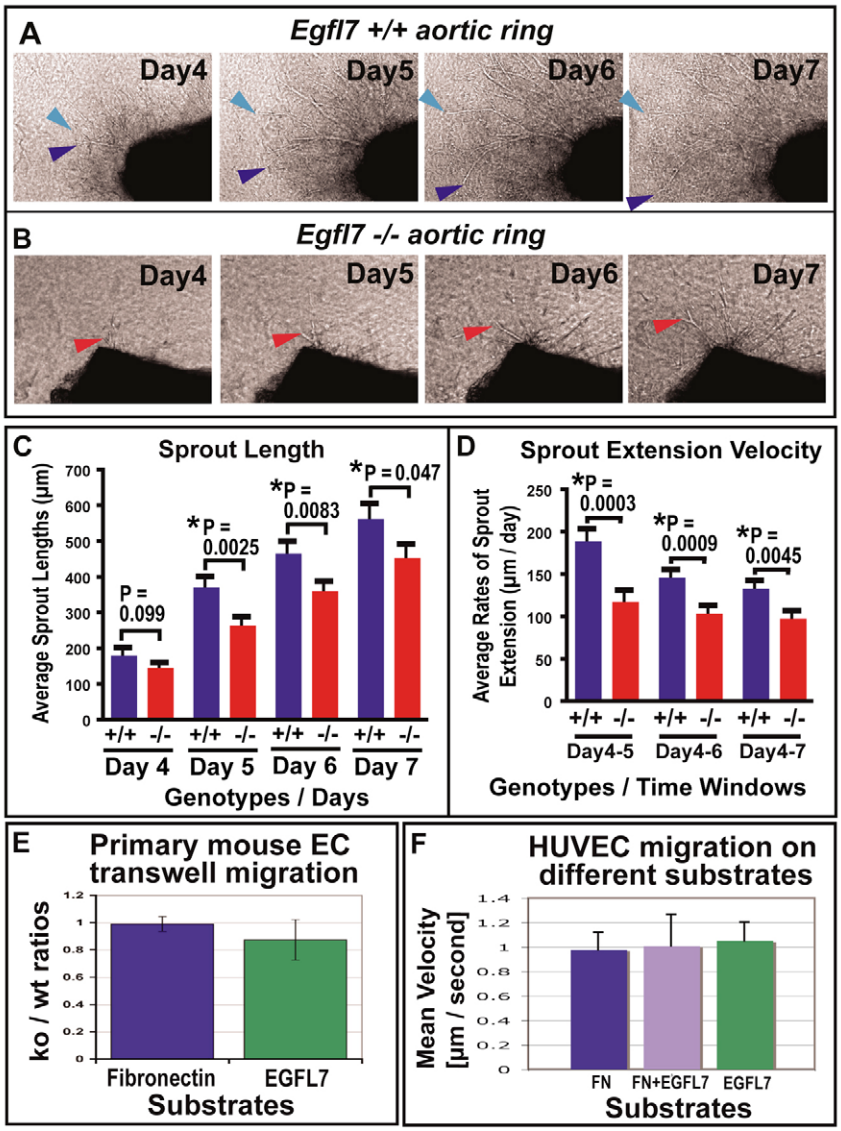

Fig. 4. EGFL7 regulates the collective migration of ECs, but not the movement of individual ECs. (**A**,**B**) Live imaging at days 4-7 of cultured mouse aortic rings isolated from *Egfl7*$^{+/+}$ (A) and *Egfl7*$^{-/-}$ (B) littermates. Colored arrowheads track individual sprouts over time. (**C**,**D**) Quantification of sprout length (C) and sprout extension velocity (D) on cultured aortic rings isolated from the *Egfl7*$^{+/+}$ (blue bars) and *Egfl7*$^{-/-}$ (red bars) littermates. (**E**) Transwell migration assay performed on fibronectin- or EGFL7-coated inserts using ECs isolated from four pairs *Egfl7*$^{+/+}$ and *Egfl7*$^{-/-}$ littermates. Migration efficiency was compared between *Egfl7*$^{-/-}$ (ko) and *Egfl7*$^{+/+}$ (wt) samples and the ratios plotted. (**F**) Migration velocity of individual HUVECs on fibronectin (FN), EGFL7, or combined substrate. The actual size represented by the width of the panel: 1.09 mm (A); 0.73 mm (B).

material). The reduced FAK phosphorylation was not due to decreased expression of FAK because total FAK staining was not altered in the *Egfl7*$^{-/-}$ tissues (see Fig. S8E-H,M-P in the supplementary material).

These two lines of evidence suggest that EC migration during sprouting angiogenesis is defective in the absence of EGFL7. Therefore, we went on to examine whether the *Egfl7*$^{-/-}$ cells have any intrinsic migratory deficit using ECs isolated from the *Egfl7*$^{+/+}$ and *Egfl7*$^{-/-}$ tissues, and compared their ability to migrate on either a fibronectin- or EGFL7-coated surface in response to VEGF stimulation. No statistically significant difference was seen between the two genotypes (Fig. 4E), indicating that the migratory machinery is intact in the *Egfl7* mutant ECs, and that they can migrate efficiently on a substrate devoid of EGFL7, such as that with fibronectin alone.

We then investigated whether the inclusion of EGFL7 in the ECM can alter the migration speed of individual ECs. To this end, we cultured HUVECs on fibronectin alone, EGFL7 alone, or a mixture of fibronectin and EGFL7, and monitored their migration using time-lapse microscopy. The migration speeds of individual ECs did not differ on these substrates (Fig. 4F).

Taken together, our data suggest that EGFL7 does not influence the migratory capacity of individual ECs, nor does it affect the ability of the ECM to support individual EC migration. Instead, EGFL7 is required for the effective movement of a cohort of ECs that migrate together.

EGFL7 regulates EC organization in angiogenic sprouts

In an attempt to understand why collective EC movement is impaired in sprouting angiogenesis, we took a closer look at the structures of angiogenic sprouts in the *Egfl7*-knockout tissues.

Sprouting is achieved through the coordinated activities of two subtypes of ECs: the chemosensing activity and motility of tip cells determine the direction of migration, whereas proliferation and unidirectional movement of the stalk cells contribute to the extension of a sprout (Gerhardt and Betsholtz, 2005). We first examined these two cell populations on wholemount retinas stained for EC and nuclear markers (Fig. 5A-F). Tip cells were present at the vascular migration front in the *Egfl7*$^{-/-}$ retinas, and the morphology of their filopodia was similar to that of the wild-type cells. In addition, the overall direction of the tip cell filopodia

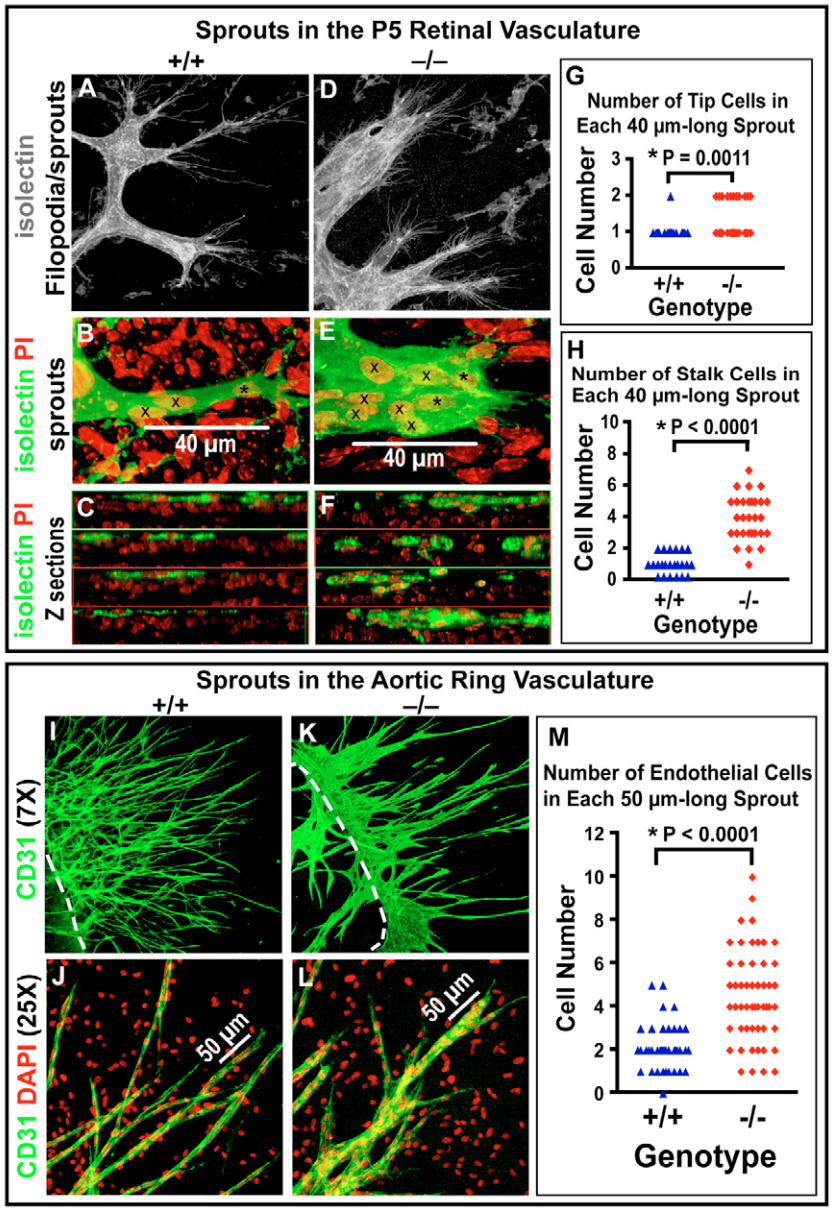

Fig. 5. EGFL7 restricts the spatial distribution of migrating ECs. (**A-F**) Confocal images of vascular sprouts in P5 retinas from *Egfl7*$^{+/+}$ (A-C) and *Egfl7*$^{-/-}$ (D-F) littermates stained with Isolectin B4 (white in A,D; green in B,C,E,F) and propidium iodide (PI) to indicate nuclei (red in B,C,E-F). C and F are *z*-sections of the retinal vascular migration front. These images were taken from areas similar to those indicated by the arrows and arrowheads in Fig. 2J,M. Crosses mark stalk cell nuclei; asterisks mark tip cell nuclei. (**G**,**H**) Tip (G) and stalk (H) cell counts in multiple 40 μm-long segments of sprouts from both genotypes. (**I-L**) Aortic rings isolated from *Egfl7*$^{+/+}$ (I,J) and *Egfl7*$^{-/-}$ (K,L) littermates stained for CD31 (green) and with DAPI (red, pseudo color). White dashed lines outline the edges of the aortic rings. The CD31^{-} DAPI^{+} signals in J and L are nuclei of fibroblasts and smooth muscle cells that have migrated away from the aortic rings. (**M**) EC counts in multiple 50 μm-long segments of sprouts from both genotypes. The actual size represented by the width of the panel: 230 μm (A,D); 76 μm (B,E); 298 μm (C,F); 1.3 mm (I,K); 294 μm (J-L).

was similar in the *Egfl7*$^{-/-}$ and *Egfl7*$^{+/+}$ tissues (Fig. 5A,D), implying that they are sensing the chemoattractant appropriately and are motile. However, when we examined the spatial distribution of the tip and stalk cells within a single sprout, we saw a striking difference between the *Egfl7*$^{-/-}$ and *Egfl7*$^{+/+}$ littermates. In the wild-type retinas, most sprouts were of similar size, with each sprout consisting of 1-2 stalk cells following a single tip cell (Fig. 5B,G,H). When examined by confocal optical sectioning along the vitreal-choroidal axis, almost all tip cells and the majority of stalk cells were always arranged in a single cell layer (Fig. 5C). In the *Egfl7*$^{-/-}$ retina, however, some tip cells and the majority of stalk cells were seen to line up in multiple cell layers along the vitreal-choroidal axis (Fig. 5E,F), producing markedly enlarged sprouts with increased tip and stalk cell numbers (Fig. 5G,H). This phenotype was most profound at P2, and partially resolved by P8.

We also examined sprout structure in cultured aortic rings isolated from *Egfl7*$^{+/+}$ and *Egfl7*$^{-/-}$ littermates. In all the *Egfl7*$^{+/+}$ rings (n=7 mice), a large number of sprouts were formed on the edge of each ring (Fig. 5I,J), and the majority of the sprouts comprised 1-2 cells across their widths, with 1-5 cells in the 50 μm-long end-segment of each sprout (Fig. 5M). In rings from 80% of the *Egfl7*$^{-/-}$ animals (n=5 mice), larger and shorter sprouts, as well as sheets of ECs, extended from the edges of the mutant rings (Fig. 5K), and there were more mutant sprouts growing over the rings, instead of away from the rings (Fig. 5K, sprouts within areas demarcated by white dashed lines). The enlargement of sprouts was evident as most of the sprouts contained many more cells in their 50 μm-long end-segments (Fig. 5L,M).

As mentioned above, similar aberrant EC clusters were seen in many *Egfl7*$^{-/-}$ tissues (arrowheads in Fig. 2 and Fig. S3 in the supplementary material). These aggregates are reminiscent of the midline angioblast aggregates seen in the *egfl7*-knockdown zebrafish embryos (Parker et al., 2004).

These observations led us to propose that EGFL7 plays a role in regulating the spatial distribution of ECs, thereby limiting the sprout size. This activity is necessary for the efficient outgrowth of nascent vessels.

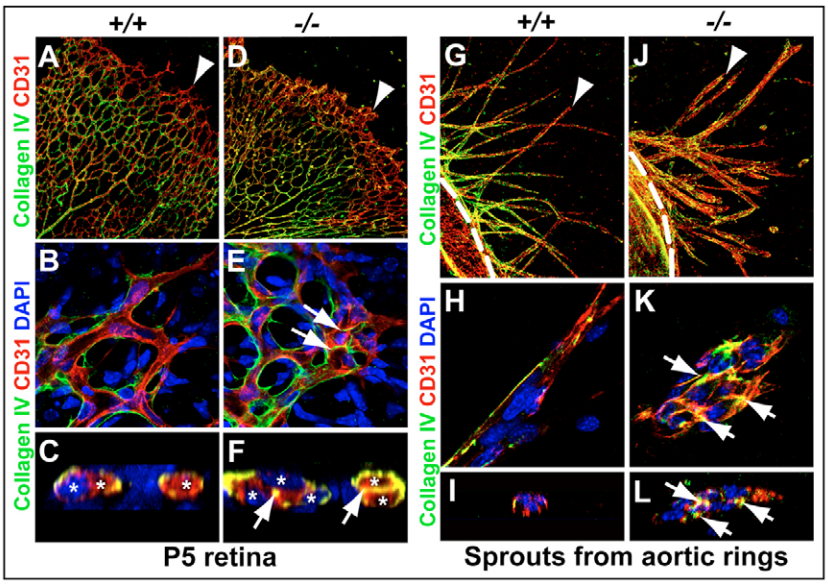

Fig. 6. Aberrant localization of basement membrane marker in the *Egfl7*$^{-/-}$ vessels. Neonatal mouse retinas (**A-F**) or aortic rings (**G-L**) isolated from the *Egfl7*$^{+/+}$ (A-C,G-I) and *Egfl7*$^{-/-}$ (D-F,J-L) littermates stained for collagen IV (green), CD31 (red) and with DAPI (blue). Representative single-frame confocal images (A,B,D,E,G,H,J,K) and optical *z*-sections (C,F,I,L) are shown. Arrowheads, vascular sprouts similar to those shown at higher magnification in the panels beneath; arrows, mislocalized collagen IV between ECs within a single sprout; asterisks, individual ECs. In C and F, two separate *z*-sections are shown in each panel. The actual size represented by the width of the panel: 732 μm (A,D); 108 μm (B,E); 36 μm (C,F); 366 μm (G,J); 72 μm (H,I,K,L).

The *Egfl7* mutant ECs fail to respect the boundary of nascent sprouts

We went on to investigate how EGFL7 regulates sprout size. The multicellular nature of the aggregates suggests that ECs might fail to recognize the boundary of nascent sprouts. To explore this possibility, we stained neonatal retinas and cultured aortic rings for collagen IV, which is a component of the vascular basement membrane.

In the *Egfl7*$^{+/+}$ neonatal retinas, collagen IV marked a portion of the basal surface of each nascent vessel at the migration front and was never present between ECs in the same sprouts (Fig. 6A-C). However, in the *Egfl7*$^{-/-}$ retinas, collagen IV was detected between ECs, especially in the centers of the enlarged sprouts (Fig. 6D-F, arrows). A similar finding was made in the cultured aortic rings isolated from a set of *Egfl7*$^{+/+}$ (Fig. 6G-I) and *Egfl7*$^{-/-}$ mice (Fig. 6J-L).

These observations suggest that *Egfl7*$^{-/-}$ ECs are unable to position themselves properly because they fail to recognize the orientation of their endothelial neighbors. However, based on the following observations, we believe that these mutant ECs can establish proper basal-luminal polarity: (1) in adult tissues, although many aberrantly associated vessels are present (Fig. 3, arrows), these vessels have lumen as indicated by fluorescein perfusion (Fig. 3C); (2) collagen IV is localized to the basal surface even in abnormally juxtaposed vessels (Fig. 3L). Therefore, EGFL7 is probably not essential for establishing polarity, but may play a role in reinforcing it.

EGFL7 is associated with the interstitial ECM

In order to understand the molecular mechanism of the phenotypes described above, we analyzed the biochemical properties of EGFL7 in vitro. When overexpressed in fibroblasts, abundant EGFL7 was detected in the ECM and cell lysates, but very little could be detected in the conditioned media even when cells were treated with high salt (Fig. 7A), indicating that EGFL7 is tightly associated with the ECM and therefore does not diffuse freely.

Surprisingly, overexpression in fibroblasts resulted in significantly more efficient deposition of EGFL7 into the ECM than in epithelial cells (data not shown). This prompted us to examine whether factor(s) produced by the fibroblasts facilitate the deposition of EGFL7 into the ECM. We cultured HUVECs alone, or in direct contact with fibroblasts. In a pure HUVEC culture, EGFL7 deposition into the ECM was a slow process, as only very low levels of EGFL7 could be detected at day 3 (Fig. 7C), and moderate levels of EGFL7 in a fibrous network could only be detected at day 6 (data not shown). This temporal profile coincided with the deposition of other ECM proteins, such as fibronectin, by HUVECs (data not shown). However, when HUVECs were cultured with human dermal fibroblasts – a cell line negative for EGFL7 (Fig. 7E) – abundant extracellular EGFL7 was detected within 3 days (Fig. 7B), indicating that fibroblasts expedite the deposition of EGFL7. We then asked whether the fibroblast activity requires direct cell-cell contact by performing co-culture of HUVECs with fibroblasts in a trans-well setting in which the two cell types are separated. We found that the kinetics of EGFL7 deposition was unchanged in the trans-well co-culture (Fig. 7D) compared with HUVEC alone (Fig. 7C), suggesting that the activity of fibroblasts requires direct contact. Similar observations were made with other interstitial cell types such as astrocytes and vascular smooth muscle cells (data not shown). Based on these observations, and the fact that fibroblasts and other interstitial cell types usually produce a greater diversity and quantity of ECM proteins than epithelial or endothelial cells, we went on to investigate whether certain ECM proteins can facilitate the deposition of EGFL7. Interestingly, we found that fibronectin and type I collagen, which belong to the subtype of matrix proteins encountered by nascent vessels when they invade new tissues (Kalluri and Zeisberg, 2006), facilitate EGFL7 deposition (Fig. 7F and data not shown), whereas laminin and type IV collagen, components of the basement membrane (Kalluri and Zeisberg, 2006), do not (Fig. 7G and data not shown).

These experiments indicate that EGFL7 is a matrix-associated protein, and its secretion and/or incorporation into the matrix depends on interstitial ECM component(s). In agreement with this, we found that EGFL7 always localizes on the basal side of ECs, and has significant overlap with fibronectin (Fig. 7H-J). Interestingly, a continuous layer of EGFL7 was found surrounding stalk cells in an angiogenic sprout (Fig. 7J), whereas only patchy EGFL7 signal was seen around tip cells (Fig. 7K). The difference in EGFL7 protein levels between tip and stalk cells might be a consequence of

accumulative secretion, as tip cells are the first ECs in a sprout to secret EGFL7 and they are constantly moving into new environments devoid of EGFL7, whereas stalk cells move into a space in which EGFL7 has already been deposited by the previous ECs migrating along the same route.

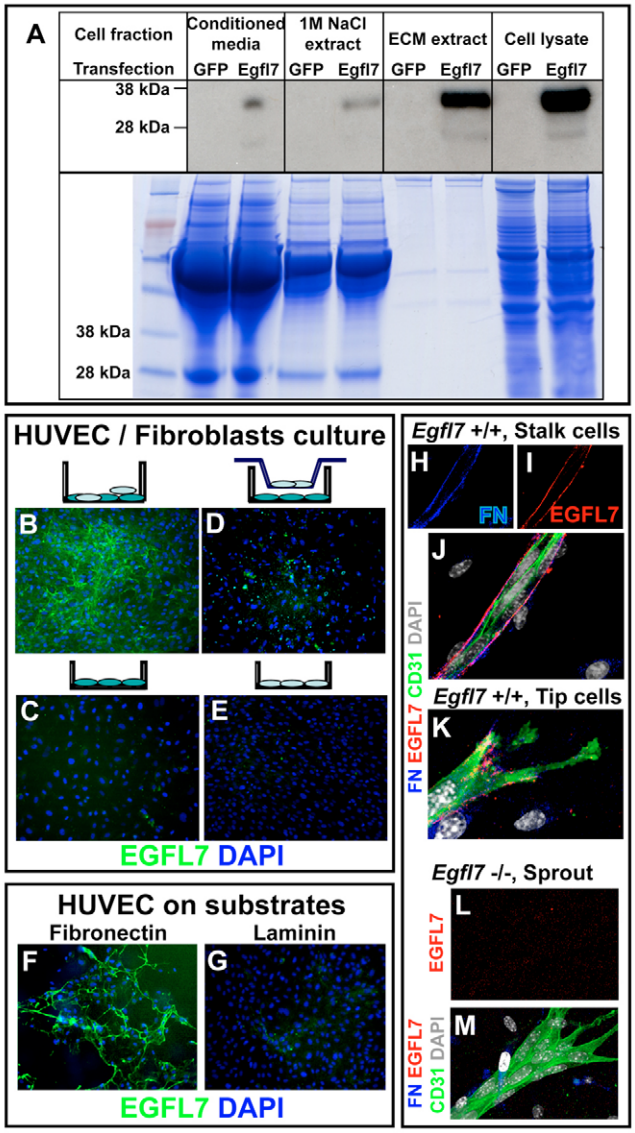

Fig. 7. EGFL7 is associated with the interstitial ECM. (**A**) Anti-HA western blot on different fractions of chicken embryonic fibroblasts expressing GFP or HA-tagged human EGFL7 (top panel), and Coomassie Blue staining of the same cell fractions prepared from an equal number of cells (bottom panel). (**B-G**) The following cells were cultured for 3 days and then double stained for EGFL7 (green) and with DAPI (blue) in the absence of detergent: HUVECs (dark blue ovals in diagram) and human dermal fibroblasts (light blue ovals) in mixed culture (B); HUVECs alone (C); fibroblasts alone (E); HUVECs in the bottom well with fibroblasts in an insert (D); or HUVEC alone on fibronectin (F) or laminin (G). (**H-M**) Confocal images of aortic ring sprouts from *Egfl7*$^{+/+}$ (H-K) or *Egfl7*$^{-/-}$ (L,M) littermates stained for fibronectin (blue), EGFL7 (red), CD31 (green) and with DAPI (gray). H-J show a segment of sprout with stalk cells; K shows tip cells; L,M show a segment of sprouts with both tip and stalk cells. The actual size represented by the width of the panel: 650 μm (B-G); 80 μm (H-J); 54 μm (K); 100 μm (L,M).

The association with the interstitial matrix suggests that EGFL7 is part of the provisional matrix that supports angiogenesis (Davis and Senger, 2005). This claim is supported by the finding that *Egfl7* expression is very low in mature vascular beds, and is upregulated during angiogenesis and vascular remodeling (Campagnolo et al., 2005; Parker et al., 2004).

EGFL7 defines an optimal path for the migrating ECs

Integrating all our findings, we propose the following model to explain how EGFL7 acts. When a nascent sprout migrates into a microenvironment surrounded by interstitial cell types capable of secreting fibrillar matrix, EGFL7 is deposited at the interface between ECs and the interstitial cells, forming a unique ECM coat on the outer surface of the sprouts. This coat delineates the boundary of a new sprout and defines an efficient migratory path for the ECs (Fig. 8A). In the absence of EGFL7, ECs fail to respect the boundary of a sprout. As a result, new ECs can attach to the basal sides of other ECs within a single sprout, or multiple sprouts can adhere to each other, thereby forming larger sprouts that cannot migrate efficiently (Fig. 8B).

DISCUSSION

Endothelial cell migration is an essential step in vascular development. Although the migration of individual EC has been extensively studied, information pertinent to how groups of ECs migrate coordinately is sparse, despite it being more relevant to vascular morphogenesis. Our study adds an element to our collective understanding of how coordinated movement is controlled.

Sprout size and collective EC migration

Our study suggests that sprout size impacts the speed of migration. To understand why, we should look at the roles played by tip and stalk cells. It is generally believed that tip cell migration and stalk cell proliferation both contribute to the extension of a sprout, and stalk cells are pulled forward by the tip cells (Gerhardt and Betsholtz, 2005; Gerhardt et al., 2003; Kurz et al., 1996; Ruhrberg et al., 2002). Our study adds an additional layer to this paradigm: under normal conditions, stalk cell proliferation may directly contribute to the forward movement of a sprout if they are lined up in a linear fashion, because the addition of a new cell will push its neighbor forward (Fig. 8A). In the *Egfl7* mutant tissues, a newly formed EC may attach to the basal side of other ECs (Fig. 8B) instead of situating side-by-side with its neighboring cells along the migratory path of the sprout (Fig. 8A); therefore, it fails to contribute to the overall forward migration.

EGFL7 and the spatial arrangement of ECs

How does EGFL7 prevent inappropriate EC association? In a previous study, we showed that EGFL7 supports EC adhesion, but their adhesive strength on EGFL7 is weaker than other matrix proteins (Parker et al., 2004). This molecular characteristic leads to our first hypothesis: as a new sprout forms, ECs within or outside of a new sprout could encounter the basal surfaces of other ECs and transiently adhere to it. However, this type of adhesion can be resolved quickly because EGFL7 modulates the adhesion strength. Without EGFL7, the adhesive strength of this inappropriate attachment might be enhanced, leading to the persistence of EC aggregation and the subsequent formation of enlarged sprouts.

Alternatively, EGFL7 could bind to a signaling molecule such as VEGF, and modulate the signaling events elicited by the signaling factor(s). This is an attractive possibility because the ECM is known

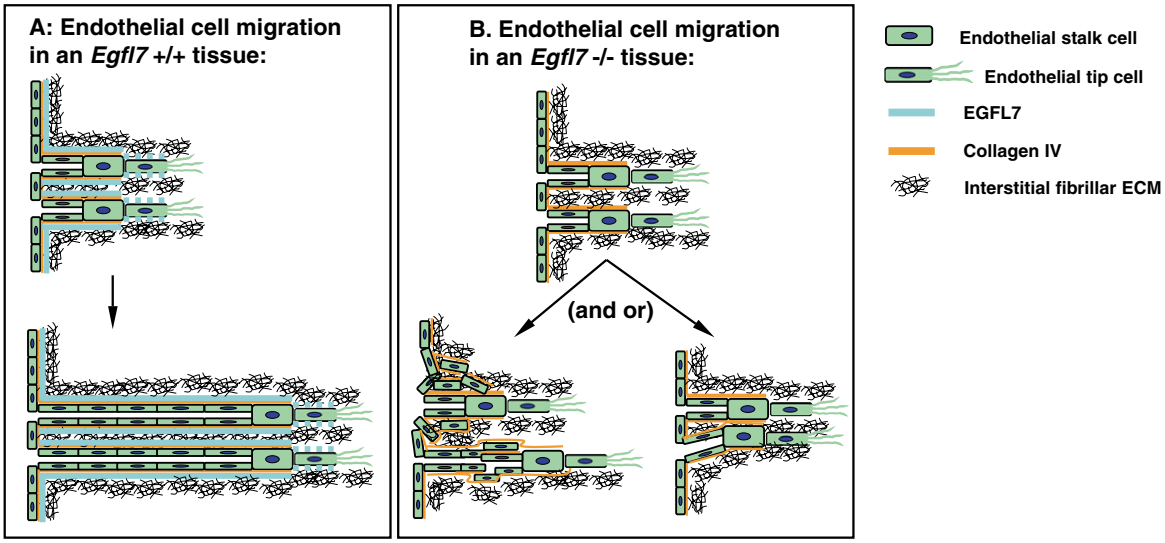

Fig. 8. A model describing how EGFL7 regulates sprout morphology and motility.

to modulate growth factor/cytokine signaling (Boudreau and Bissell, 1998). Future efforts will focus on identifying factor(s) that are potentially modulated by EGFL7.

Partial recovery from the early abnormality

Despite the formation of EC aggregates in many mutant vascular beds, functional vasculatures are formed later in development. There are several possibilities as to how the structural abnormalities could be corrected. (1) Multiple lumens could form within the EC aggregates. This hypothesis is supported by the presence of the multivessel structures in adult tissues (Fig. 3). (2) The ectopic cells in the aggregates might be eliminated at a later stage when the vasculature is perfused, presumably owing to lack of trophic support from shear stress (Li et al., 2005). (3) Delayed vascular development might trigger the production of a strong migration factor that stimulates the aggregated ECs to migrate away. The presence of abnormal structures in adult vasculatures indicates that the recovery is not a complete correction of the early problems.

Embryonic lethality

In this study, although we have not identified the exact cause of embryonic lethality in the *Egfl7* mutant lines, we believe that the vascular developmental defects probably contribute to the cause. The percentages of embryos with delayed coronary vascular development at E14.5 (Fig. 2G) and with systemic oedema (Table 2) are both ~50%, suggesting that the coronary vascular defect might compromise circulation and lead to severe oedema and death.

Although defective blood circulation is a much more prevalent cause of oedema than lymphatic problems, we cannot exclude the possibility of lymphatic failure in the knockout embryos. We will investigate this possibility in future work.

Partial penetrance

The partial penetrance in embryonic lethality and some other phenotypic aspects is puzzling. So far, we have not identified a plausible compensatory factor. It is possible that a genetic modifier exists, but it is probably a weak modifier based on the following observation: in the N10 C57Bl/6 mice, there is a trend toward further reduction of viable $Egfl7^{-/-}$ mice compared with N5 C57Bl/6 mice, but the difference is not yet statistically significant (P=0.0921, Table 1). An alternative possibility is that the partial penetrance is due to a threshold effect and is stochastic in nature.

Implications

The ECM influences many steps in vascular development (Brooke et al., 2003; Davis and Senger, 2005; Whelan and Senger, 2003); however, the specific mechanism through which each matrix component influences the behavior of ECs is only partially understood. In this report, we have used EGFL7 as an example to demonstrate that a single ECM component can play a unique role in angiogenesis. Our study illustrates that vascular development is a complex process orchestrated by many molecular players, including each constituent of the ECM.

We thank the following colleagues for their excellent technical support and advice: Judy Young, Kristin Harden, Dan Eaton, Jean Starks, Shannon Liu, Zhenyu Gu, Christine Olson, Ellen Filvaroff, Jun Li, Fred de Sauvage, Jed Ross, Nick van Bruggen, Racquel Corpuz, Richard Vandlen, Hok-Seon Kim; Dan Yansura at Genentech; Suzanne van Dijk, René Scriwanek and Marc van Peski at the University Medical Center, Utrecht; and Diane Markesich at Lexicon Genetics. We thank Drs Leon Parker, Harald Junge and Grant Kalinowski for their critical reading of the manuscript.

Supplementary material

Supplementary material for this article is available at
http://dev.biologists.org/cgi/content/full/134/16/2913/DC1

References

Benjamin, L. E., Hemo, I. and Keshet, E. (1998). A plasticity window for blood vessel remodelling is defined by pericyte coverage of the preformed endothelial network and is regulated by PDGF-B and VEGF. *Development* **125**, 1591-1598.

Boudreau, N. and Bissell, M. J. (1998). Extracellular matrix signaling: integration of form and function in normal and malignant cells. *Curr. Opin. Cell Biol.* **10**, 640-646.

Brooke, B. S., Karnik, S. K. and Li, D. Y. (2003). Extracellular matrix in vascular morphogenesis and disease: structure versus signal. *Trends Cell Biol.* **13**, 51-56.

Campagnolo, L., Leahy, A., Chitnis, S., Koschnick, S., Fitch, M. J., Fallon, J. T., Loskutoff, D., Taubman, M. B. and Stuhlmann, H. (2005). EGFL7 is a chemoattractant for endothelial cells and is up-regulated in angiogenesis and arterial injury. *Am. J. Pathol.* **167**, 275-284.

Carmeliet, P. and Tessier-Lavigne, M. (2005). Common mechanisms of nerve and blood vessel wiring. *Nature* **436**, 193-200.

Coultas, L., Chawengsaksophak, K. and Rossant, J. (2005). Endothelial cells and VEGF in vascular development. *Nature* **438**, 937-945.

Davis, G. E. and Senger, D. R. (2005). Endothelial extracellular matrix:

biosynthesis, remodeling, and functions during vascular morphogenesis and neovessel stabilization. *Circ. Res.* **97**, 1093-1107.
Dorrell, M. I. and Friedlander, M. (2006). Mechanisms of endothelial cell guidance and vascular patterning in the developing mouse retina. *Prog. Retin. Eye Res.* **25**, 277-295.
Eichmann, A., Makinen, T. and Alitalo, K. (2005). Neural guidance molecules regulate vascular remodeling and vessel navigation. *Genes Dev.* **19**, 1013-1021.
Fiore, R., Rahim, B., Christoffels, V. M., Moorman, A. F. and Puschel, A. W. (2005). Inactivation of the Sema5a gene results in embryonic lethality and defective remodeling of the cranial vascular system. *Mol. Cell. Biol.* **25**, 2310-2319.
Fitch, M. J., Campagnolo, L., Kuhnert, F. and Stuhlmann, H. (2004). Egfl7, a novel epidermal growth factor-domain gene expressed in endothelial cells. *Dev. Dyn.* **230**, 316-324.
Flamme, I., Frolich, T. and Risau, W. (1997). Molecular mechanisms of vasculogenesis and embryonic angiogenesis. *J. Cell. Physiol.* **173**, 206-210.
Friedl, P., Hegerfeldt, Y. and Tusch, M. (2004). Collective cell migration in morphogenesis and cancer. *Int. J. Dev. Biol.* **48**, 441-449.
Gerhardt, H. and Betsholtz, C. (2005). How do endothelial cells orientate? *EXS* **94**, 3-15.
Gerhardt, H., Golding, M., Fruttiger, M., Ruhrberg, C., Lundkvist, A., Abramsson, A., Jeltsch, M., Mitchell, C., Alitalo, K., Shima, D. et al. (2003). VEGF guides angiogenic sprouting utilizing endothelial tip cell filopodia. *J. Cell Biol.* **161**, 1163-1177.
Haas, P. and Gilmour, D. (2006). Chemokine signaling mediates self-organizing tissue migration in the zebrafish lateral line. *Dev. Cell* **10**, 673-680.
Kalluri, R. and Zeisberg, M. (2006). Fribroblasts in cancer. *Nat. Rev. Cancer* **6**, 392-401.
Kidd, K. R. and Weinstein, B. M. (2003). Fishing for novel angiogenic therapies. *Br. J. Pharmacol.* **140**, 585-594.
Kurz, H., Gartner, T., Eggli, P. S. and Christ, B. (1996). First blood vessels in the avian neural tube are formed by a combination of dorsal angioblast immigration and ventral sprouting of endothelial cells. *Dev. Biol.* **173**, 133-147.
Lavine, K. J., White, A. C., Park, C., Smith, C. S., Choi, K., Long, F., Hui, C. C. and Ornitz, D. M. (2006). Fibroblast growth factor signals regulate a wave of Hedgehog activation that is essential for coronary vascular development. *Genes Dev.* **20**, 1651-1666.
Li, Y. S., Haga, J. H. and Chien, S. (2005). Molecular basis of the effects of shear stress on vascular endothelial cells. *J. Biomech.* **38**, 1949-1971.
Parker, L. H., Schmidt, M., Jin, S. W., Gray, A. M., Beis, D., Pham, T., Frantz, G., Palmieri, S., Hillan, K., Stainier, D. Y. et al. (2004). The endothelial-cell-derived secreted factor Egfl7 regulates vascular tube formation. *Nature* **428**, 754-758.
Parsons, J. T. (2003). Focal adhesion kinase: the first ten years. *J. Cell Sci.* **116**, 1409-1416.
Patan, S. (2004). Vasculogenesis and angiogenesis. *Cancer Treat. Res.* **117**, 3-32.
Rembold, M., Loosli, F., Adams, R. J. and Wittbrodt, J. (2006). Individual cell migration serves as the driving force for optic vesicle evagination. *Science* **313**, 1130-1134.
Rice, D. S., Huang, W., Jones, H. A., Hansen, G., Ye, G. L., Xu, N., Wilson, E. A., Troughton, K., Vaddi, K., Newton, R. C. et al. (2004). Severe retinal degeneration associated with disruption of semaphorin 4A. *Invest. Ophthalmol. Vis. Sci.* **45**, 2767-2777.
Rossant, J. and Howard, L. (2002). Signaling pathways in vascular development. *Annu. Rev. Cell Dev. Biol.* **18**, 541-573.
Ruhrberg, C., Gerhardt, H., Golding, M., Watson, R., Ioannidou, S., Fujisawa, H., Betsholtz, C. and Shima, D. T. (2002). Spatially restricted patterning cues provided by heparin-binding VEGF-A control blood vessel branching morphogenesis. *Genes Dev.* **16**, 2684-2698.
Soncin, F., Mattot, V., Lionneton, F., Spruyt, N., Lepretre, F., Begue, A. and Stehelin, D. (2003). VE-statin, an endothelial repressor of smooth muscle cell migration. *EMBO J.* **22**, 5700-5711.
Stone, J., Itin, A., Alon, T., Pe'er, J., Gnessin, H., Chan-Ling, T. and Keshet, E. (1995). Development of retinal vasculature is mediated by hypoxia-induced vascular endothelial growth factor (VEGF) expression by neuroglia. *J. Neurosci.* **15**, 4738-4747.
Whelan, M. C. and Senger, D. R. (2003). Collagen I initiates endothelial cell morphogenesis by inducing actin polymerization through suppression of cyclic AMP and protein kinase A. *J. Biol. Chem.* **278**, 327-334.
Yancopoulos, G. D., Davis, S., Gale, N. W., Rudge, J. S., Wiegand, S. J. and Holash, J. (2000). Vascular-specific growth factors and blood vessel formation. *Nature* **407**, 242-248.
Zambrowicz, B. P., Friedrich, G. A., Buxton, E. C., Lilleberg, S. L., Person, C. and Sands, A. T. (1998). Disruption and sequence identification of 2,000 genes in mouse embryonic stem cells. *Nature* **392**, 608-611.
Zambrowicz, B. P., Abuin, A., Ramirez-Solis, R., Richter, L. J., Piggott, J., BeltrandelRio, H., Buxton, E. C., Edwards, J., Finch, R. A., Friddle, C. J. et al. (2003). Wnk1 kinase deficiency lowers blood pressure in mice: a gene-trap screen to identify potential targets for therapeutic intervention. *Proc. Natl. Acad. Sci. USA* **100**, 14109-14114.